




Nanosphere Photolithography: The Influence of Nanopore Arrays Disorder on Extraordinary Optical Transmission

Andrei Ushkov^{1,2}^a, Olivier Dellea³, Isabelle Verrier¹, Thomas Kampfe¹, Alexey Shcherbakov⁴^b, Jean-Yves Michalon¹ and Yves Jourlin¹^c

¹Univ. Lyon, UJM-Saint-Etienne, CNRS, Institut d'Optique Graduate School, Laboratoire Hubert Curien UMR 5516, F-42023 Saint-Etienne, France

²Center for Photonics and 2D Materials, Moscow Institute of Physics and Technology, 9 Institutsky Lane, Dolgoprudny 141700, Russia

³Grenoble Alpes Univ., CEA-Liten, 17 rue des Martyrs, 38054 Grenoble, France

⁴Department of Physics and Engineering, ITMO University, 49 Kronverksky Pr., 197101 St. Petersburg, Russia

Keywords: Nanosphere Photolithography, NPL, Extraordinary Optical Transmission, EOT, Disorder, Nanopore Array, Diffraction Grating, Plasmonics, Numerical Simulations.

Abstract: We analyze both experimentally and numerically the influence of nanopore arrays disorder on extraordinary optical transmission in samples, fabricated via nanosphere photolithography. Two measures of disorder are considered, the correlations between them are discussed using experimental and numerical data. We propose a theoretical model which takes explicitly the disorder into account, and show how the concurrence between nanopore depth and disorder level defines the quality of EOT excitation. Simulated spectra are in a good agreement with experimental ones. Our results reveal the possibilities of NPL for EOT-based applications and pave the way toward plasmonic devices with a polycrystalline design.


1 INTRODUCTION


Since its discovery in 1998 by Ebbesen (Ebbesen et al., 1998), the Extraordinary Optical Transmission (EOT) has been studied intensively for numerous applications in optical filtering (Wen et al., 2019), sensing (Yeh et al., 2011) and energy transfer (Andrew and Barnes, 2004). Different EOT-compatible sample designs were considered, for example continuous or perforated thin metal films (Ushkov et al., 2019; Jourlin et al., 2009; Sauvage-Vincent et al., 2013; Wen et al., 2019; Park et al., 2020; Yue et al., 2014), metallic slit arrays (Deng et al., 2018), deep undulations for localized plasmon excitations (Genet and Ebbesen, 2010). In order to fabricate samples and study the EOT experimentally, various surface nanostructuring approaches exist: Electron-Beam Lithography (Li et al., 2010; Yue et al., 2014), Focused Ion Beam Milling (Ebbesen et al., 1998; Hahn et al., 2020; Liu et al., 2020b), Soft-Nanoimprinting (Cam-


pos et al., 2008) or Laser Interference Lithography (Ushkov et al., 2020; Cao et al., 2018).

Nowadays the self-assembled colloidal monolayers attract more and more attention for practical plasmonic applications. Despite the polycrystalline geometry, structures fabricated via colloidal self-assembly can support resonant optical effects. Plasmon-mediated resonant transmission was observed, for example, in samples prepared via metal deposition into the interstices between colloidal particles (Liu et al., 2020a; Jamiolkowski et al., 2019), or in continuous metal films covering a self-assembled nanosphere mask (Farcau, 2019; Quint and Pacholski, 2014; Zhang et al., 2012) with or without the removal of particles.

The deposition of close-packed self-assembled colloidal monolayers on different substrates is performed by various modifications of the Langmuir-Blodgett technique (Ruan et al., 2007; Delléa et al., 2014; Lotito and Zambelli, 2016; Vogel et al., 2011). In comparison with conventional periodic structuration methods these approaches possess a high throughput, are well adapted for the curved and non-conventional surfaces (Berthod et al., 2017; Pen-

^a <https://orcid.org/0000-0001-8962-1599>

^b <https://orcid.org/0000-0002-9070-5439>

^c <https://orcid.org/0000-0002-7935-2150>

dergraph et al., 2013; Bhawalkar et al., 2010) and can be integrated into industrial production lines (Delléa et al., 2014).

The disorder should be explicitly taken into account for the polycrystalline structures. It was shown both numerically and experimentally (Quint and Pacholski, 2014) that the disorder in thin gold film undulations flattens and lowers the optical transmission; the randomness in film perforation positions leads to a broadband absorption (Fang et al., 2015), polycrystalline structures were used as light absorbers (Qu and Kinzel, 2016).

In this work we study the influence of disorder on EOT in samples, prepared via an advanced surface nanostructuring method called Nanosphere Photolithography (NPL) (Zhang et al., 2016). In contrast to other colloidal-based approaches mentioned above, NPL is much more flexible in the nanotopography as it employs photonic nanojets for drawing surface motifs. This feature makes it possible to control the surface undulations depth, avoid the photoresist layer perforations and produce nanopores - the geometry more flexible for the tuning of plasmonic response in comparison with nanoholes (Gartia et al., 2013; Wang et al., 2013). We consider two measures of nanopore arrays disorder, compare them and show how to explicitly take the disorder into account in numerical simulations. Experimental EOT measurements are in a good correspondence with calculated spectra. In addition, we propose a phenomenological model, adapted from the 1D case (Nau et al., 2007), for EOT calculations in disordered 2D structures. Our results are promising to reveal the possibilities of NPL for EOT-based applications and pave the way toward plasmonic devices with a polycrystalline design.

2 FABRICATION AND CHARACTERIZATION OF SAMPLES

In Fig. 1 we present the main technological steps for samples fabrication. On a surface of BK7 glass slides 3.7×2.5 cm, cleaned in ultrasonic acetone, ethanol baths and DI-water bath, a 600 nm/250 nm-thick Shipley S1805 photoresist layer is spin-coated for $1.1 \mu\text{m}/300$ nm microsphere diameter, respectively, see Fig. 1a. The resist was soft-baked at 60°C for 1 min. The Boostream process, developed in CEA-Liten (Delléa et al., 2014), performs the self-assembly of silica nano/micro particles with diameters of $\sigma_0 = 1.1 \mu\text{m}$ or 300 nm into close-packed monolayers on the water surface. The Boostream

process allows the transfer of these polycrystalline monolayers onto the substrate in a continuous manner, which is advantageous for industrial needs (Shavdina et al., 2015). The colloidal mask on the resist surface acts as a microlens array for UV irradiation (see Fig. 1b) and exposes the resist during a certain time $t_{\text{exp}} \sim 10$ s. The exposed sample is then cleaned in an ultrasonic bath from the colloidal particles and is developed in MF-319 developer at 8°C for $t_{\text{dev}} \sim 4$ s. As a result, nanopore arrays appear in the resist, see Fig. 1c. Final fabrication steps (Figs. 1d-e) are 20 nm-thick aluminum layer deposition via magnetron sputtering, and the second 600 nm-thick resist coating to protect the metal and create the symmetrical "Insulator-Metal-Insulator" (IMI) structure with improved EOT behavior.

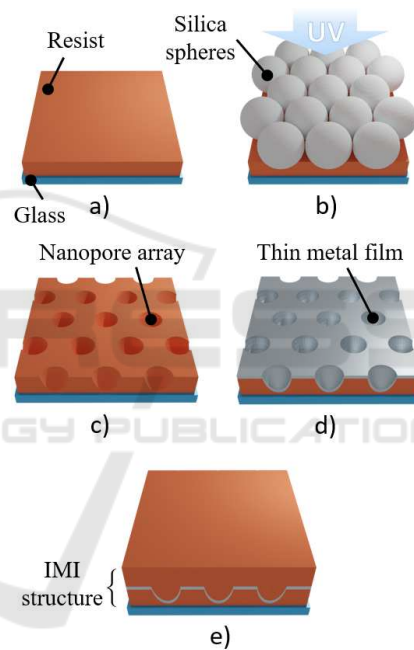


Figure 1: Nanopore array fabrication: a) The glass slide cleaning and a deposition of a photoresist film; b) deposition of colloidal monolayer, UV irradiation; c) the removal of colloidal particles, resist development and formation of nanopores; d) surface metallization; e) second resist film deposition for the symmetrical "Insulator-Metal-Insulator" (IMI) structure.

An optical microscope and SEM were used to visualize arrays with inter-pore distances $1.1 \mu\text{m}$ and 300 nm, respectively, before the final resist coating in Fig. 1e. Four samples S1-S4 were fabricated experimentally with different inter-pore distances and disorder, see Figs. 2a-d. Nanopore depth was measured using AFM, transmission spectra of IMI structures were measured using the UV/Vis/NIR spectrophotometer Cary 5000.

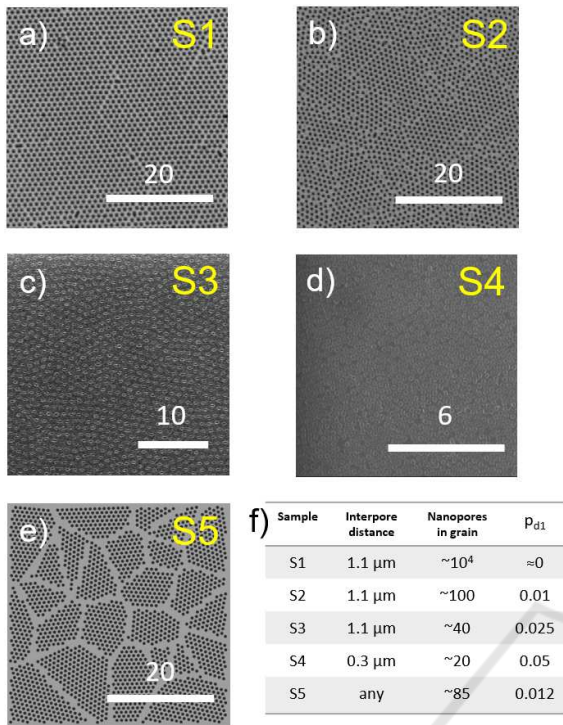


Figure 2: a)-c) Optical microscope photographs of NPL-fabricated nanopore arrays samples S1-S3 with different quality and a mean interpore distance $\sigma_0 = 1.1 \mu\text{m}$. AFM-measured nanopore depth is $\sim 220 \text{ nm}$; d) SEM photograph of nanopore sample S4 with a mean interpore distance $\sigma_0 = 300 \text{ nm}$, AFM-measured nanopore depth 50 nm ; e) Example of simulated polycrystalline sample; f) the mean interpore distance σ_0 , average number N of nanopores in grains and a measure of disorder $1/N$ for every sample S1-S5. Values above the scale bars in a)-e) show the distances in microns.

3 PARAMETERS OF DISORDER

In two-dimensional systems a number of parameters have been proposed to quantify the disorder: nanopore concentration and hole-to-hole spacing (Reilly III et al., 2010), impurity concentration (Gray et al., 2015), statistical control parameter (Richter et al., 2011). In this work we consider two measures of disorder p_{d1} and p_{d2} : nanopores per grain and the normalized width of the structure factor peak, respectively. In what follows these parameters are used for EOT calculations, and the correlation between them is discussed.

Numerical simulations of transmission spectra were performed using a proprietary GSMCC code (Shcherbakov and Tishchenko, 2017) and the Lumerical FDTD software. In the FDTD method nanopores have vertical walls, in the GSMCC simulations the

walls were slightly slanted. Both methods produced similar spectra, which assures the attained numerical results. The material dispersion is used for simulations, the dispersion of the resist S1805 was measured by ellipsometry.

3.1 Nanopores Per Grain

In the context of polycrystalline geometries a natural measure of disorder is an average number N of nanopores per grain, because this value is dimensionless, allows to compare samples with different characteristic lengths and is easy to estimate from experimental data. We use the inverse number of nanopores per grain as the first of two parameters of disorder: $p_{d1} \equiv 1/N$. The values p_{d1} for the samples S1-S4, which are specified in Fig. 2f, confirm the visual impression that the disorder increases from S1 to S4. In order to clarify the nanopore distribution in high-quality samples, we performed the image-processing-based statistical analysis of large $227 \mu\text{m} \times 170 \mu\text{m}$ microscope photographs, nanopore grains with different orientations of hexagonal lattice are depicted by different colors in Fig. 5b. These photographs allow estimating an average huge number of nanopores per grain as $\sim 10^4$ by defining the grain size in S1 as $100 \mu\text{m}$. This grain size, however, is still much smaller than the spectrophotometer incident light spot $1 \text{ mm} \times 3 \text{ mm}$, so in all samples S1-S4 it measures a collective response of numerous randomly oriented domains.

Figures 3a-b show the measured transmission spectra at normal incidence through metallized samples S3 and S1, respectively. The pronounced EOT peak exists in S1 only due to its long-range order; the EOT resonant wavelength $\lambda_{EOT} \approx 1530 \text{ nm}$ can be estimated via the formula for hexagonal lattice (Ekşioğlu et al., 2016):

$$\lambda_{EOT} = \frac{\sqrt{3}\sigma_0}{2} \sqrt{\frac{\epsilon_d \cdot \text{Re}(\epsilon_m)}{\epsilon_d + \text{Re}(\epsilon_m)}}, \quad (1)$$

for 6 symmetrical first diffraction orders $(m, n) = (\pm 1, 0), (0, \pm 1), (\pm 1, \mp 1)$; ϵ_d and ϵ_m are dielectric permittivities of dielectric and metallic layers, respectively, and σ_0 is the interpore distance defined by the diameter of the self-assembled particles. Although in Fig. 3b the modeling of ideal hexagonal lattice is enough for a good correspondence with experiment, the disorder in Fig. 3a necessitates the simulation of the periodical super cell, as shown in Fig. 3a inset.

The nanopore distribution from experimental data was used in Fig. 3a, the cell size is adapted to include the mean number of nanopores per grain $N = 43$ in

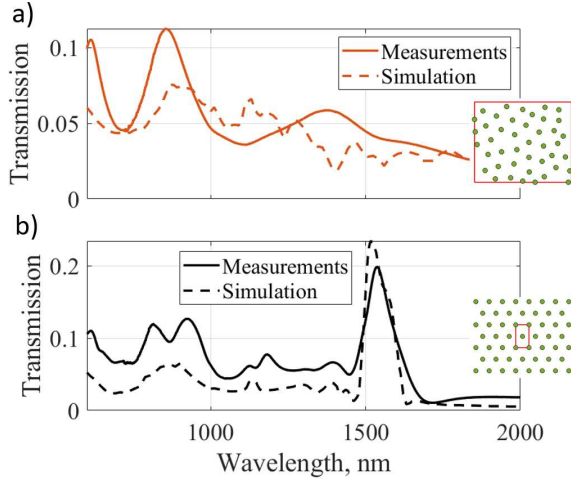


Figure 3: Transmission spectra at normal incidence with and without EOT through samples with a mean intercore distance $1.1 \mu\text{m}$. Solid curves in a) and b) correspond to the measured transmission through samples S3 and S1, respectively. Dashed lines in a) and b) are the calculated spectra of nanopore arrays arranged in periodical cells, shown as insets in a) and b); red rectangles denote periodical boundary conditions, its size in a) is $6816 \times 5636 \text{ nm}$.

correspondence with values of Fig. 2f. Both experimental and numerical results show that a high disorder in nanopore arrays effectively suppresses the EOT peak.

Although the parameter p_{d1} is easy to estimate from experimental data and allows to define properly the size of super cells with disorder, it is a geometrical value which is not directly connected with sample diffraction properties. We believe that for EOT-based devices another parameter of disorder is more appropriate, introduced in the next section.

3.2 Normalized Width of the Structure Factor Peak

As it was mentioned above, the experimental samples consist of a huge number of randomly oriented grains, illuminated by normally incident light during spectral measurements. We study the EOT caused by first diffraction orders; in polycrystalline samples these orders, coming from different grains, create a circle in reciprocal space with the radius $k_c \equiv |\mathbf{b}_1| = |\mathbf{b}_2|$, where \mathbf{b}_1 and \mathbf{b}_2 are basis reciprocal vectors for an ideal hexagonal grating, see Fig. 4. To calculate a Fourier transform $\rho_{\mathbf{k}}$ of nanopore arrays we use a set of two-dimensional Dirac delta functions $\rho(\mathbf{r}) = \sum_{i=1}^N \delta(\mathbf{r} - \mathbf{r}_i)$, which are zero except nanopore centers $\mathbf{r} = \mathbf{r}_i$, and get $\rho_{\mathbf{k}} = \sum_{i=1}^N \exp(i\mathbf{k} \cdot \mathbf{r}_i)$. The blue profile in Fig. 4 represents the radial-averaged static structure factor $S(k)$, which is proportional to

the squared modulus of Fourier amplitudes: $S(\mathbf{k}) = \langle \rho_{\mathbf{k}} \rho_{-\mathbf{k}} \rangle / N$.

If nanopore grains are large enough (as for the sample S1), the circle is thin, and the measured EOT is almost the same as for ideal hexagonal grating (see Fig. 3b), even if the total number of illuminated grains is big. The transmission through periodical hexagonal lattices weakly depends to incident light polarization due to the 6-fold rotational symmetry (Zhao et al., 2017). Our preliminary calculations show that transmission variations are well below 1% for any linear polarization in hexagonally arranged nanopores. For samples with smaller grains the reciprocal space circle is wider in analogy with diffraction in amorphous liquids (Ziman, 1979; Rojas-Ochoa et al., 2004). Consequently, the Full Width at Half Maximum (FWHM) of the radial distribution can serve as a measure of disorder, connected with the structure diffraction properties. In this paper we consider the dimensionless parameter of disorder $p_{d2} \equiv \text{FWHM}/k_c$.

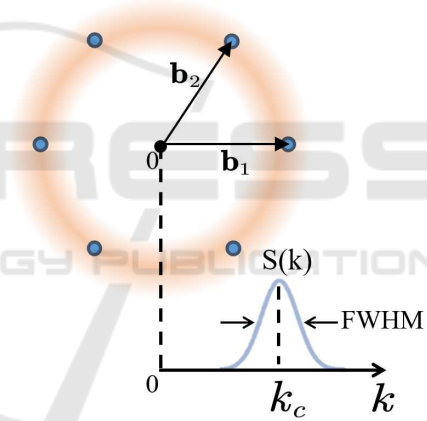


Figure 4: Sketch of the first Fourier harmonics circle for polycrystalline gratings. Reciprocal basis vectors \mathbf{b}_1 and \mathbf{b}_2 and 6 first diffraction orders denoted by blue points are defined by ideal hexagonal nanopore arrangement. The profile along the circles radius (in blue) represents the static structure factor $S(k)$.

The both parameters p_{d1} and p_{d2} grow with the growth of disorder, their values for experimental samples S1-S4 are shown in Fig. 5a. According to this figure, the reciprocal space circle slows its width growth with the increase of p_{d1} , it means that diffraction properties of structures with small crystallites do not depend sufficiently on the disorder level, in contrast to samples with large crystallites and a long-range order. In order to understand this behavior better we developed a simple model of polycrystalline nanopore arrays (see, for example, S5 in Fig. 2e). For every simulation a set of points is chosen randomly, and the Voronoi diagram of this set defines

the nanopore grains boundaries. The space inside grains is filled with hexagonally arranged elements (nanopores), the lattice orientation is chosen randomly in every grain. We leave the thin stripes along boundaries empty to avoid the overlap of nanopores from different grains. In such a way, numerous realizations of nanopore arrays with different p_{d1} were simulated, and corresponding values of p_{d2} were calculated. In Fig. 5a parameters p_{d1} and p_{d2} of individual simulated nanopore distributions are denoted, together with a phenomenological power function fitting $p_{d2}(p_{d1}) = 0.63p_{d1}^{0.45}$.

The comparison of experimental and modeled dependences $p_{d2}(p_{d1})$ in Fig. 5a allows to make two observations. Firstly, the modeled monotone function generally repeats the experimental behavior, thus the average number of nanopores per grain can, to a first approximation, determine a diffraction quality of samples. Secondly, the experimental values of p_{d2} tend to be larger than those predicted by a simple polycrystalline model. It can be explained by the presence of additional defects in nanopore arrays along with randomly oriented crystallites, i.e. hexagonal lattice phase jumps (Avrutsky et al., 2000) (white uncolored lines in Fig. 5b) and regions between grains, filled with randomly distributed nanopores. Although these defects can be introduced into the modelling, it goes beyond the scope of this paper. In the following section we use the "diffraction" parameter of disorder for numerical simulation of EOT.

3.3 Influence of Nanopore Arrays Disorder on EOT

In order to utilize the parameter p_{d2} and introduce explicitly the disorder into numerical EOT calculations we propose a model, adapted from the 1D case (Nau et al., 2007). A radial-symmetric structure factor $S(k)$, calculated for experimental nanopore distribution, is least square fitted to a Gaussian to obtain the value of p_{d2} . At the same time, the structure peak width defines a set of effective first diffraction orders k , which come from different grains and give a contribution $\alpha_k T_k(\lambda)$ to the total transmission $T(\lambda)$ at a wavelength λ . We assume a simple incoherent summation of these partial contributions because of numerous randomly oriented and distributed grains. The scaling factor α_k depends on the density of excited modes and is proportional to the corresponding value $S(k)$.

The total transmission is the sum of all partial contributions with k around the structure factor peak, where the α_k is sufficiently non-zero: $T(\lambda) = \sum_k \alpha_k T_k(\lambda)$. Partial spectra T_k are obtained from the

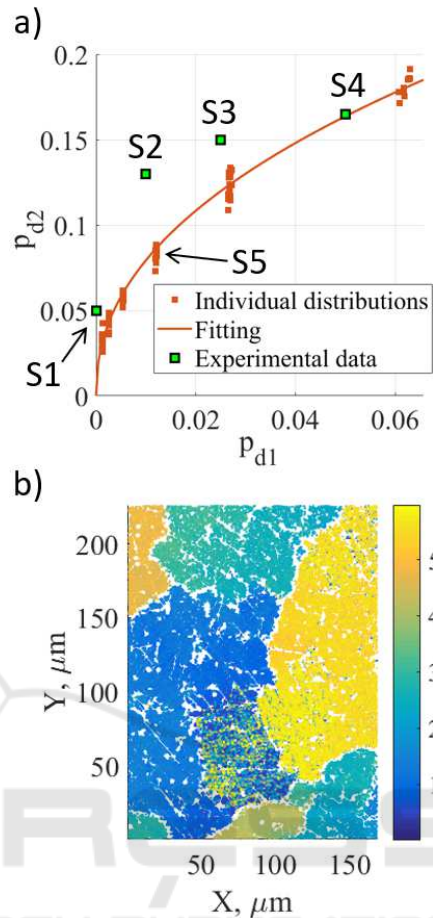


Figure 5: a) Correlation between two disorder parameters p_{d1} and p_{d2} for simulated (brown points and fitting line) and experimental nanopore distributions (green squares). Samples S1-S4 and the example of simulated distribution S5 are shown in Figs. 2a-e. The phenomenological power function fitting $p_{d2} = 0.63p_{d1}^{0.45}$ is used.

simulation of perfect samples (Nau et al., 2007).

Figure 6a shows several calculated transmission spectra at normal incidence for 50 nm-depth nanopore arrays, for different disorder levels p_{d2} . The experimentally measured value of EOT and its spectral shape for sample S4 is in a good agreement with theoretical results at appropriate disorder level, compare with its value in Fig. 5a. The "diffraction" parameter p_{d2} is convenient to study the influence of continuously varying disorder on EOT. Figure 6b demonstrates the change of maximum EOT value with nanopore depth at numerous disorder levels. Generally, the disorder suppresses the resonant transmission. Interestingly, it can also turn a transmission decreasing with a depth growth into an increasing one, for deep gratings (see the highest and the lowest curves in Fig. 6b at depth > 100 nm). The 3D-representation of calculated data in Fig. 6c re-

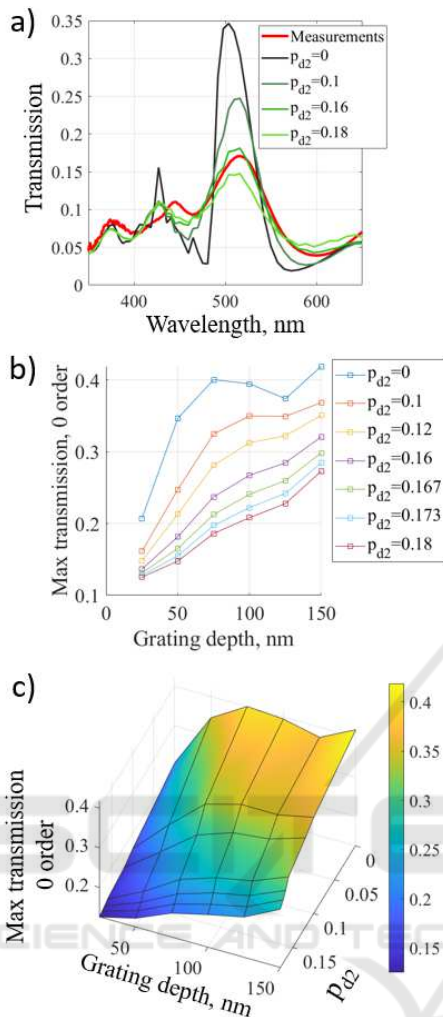


Figure 6: a) A set of calculated transmission spectra (tones of green) at normal incidence with different parameter of disorder p_{d2} . A red curve shows an experimentally measured transmission for the sample S4. Simulated and experimental nanopore depth is 50 nm; b) calculated maximum EOT transmission as a function of grating depth for a set of p_{d2} ; c) 3D-representation of data from b), showing a concurrence between grating depth and disorder for the value of EOT.

veals an interplay between grating depth and disorder for establishing a EOT value.

4 CONCLUSIONS

In conclusion, we analyzed both experimentally and numerically the influence of nanopore arrays disorder on extraordinary optical transmission in samples, fabricated via nanosphere photolithography. We used two measures of disorder: "geometrical" parameter p_{d1} and "diffraction" parameter p_{d2} , and constructed a

simple model of nanopore distributions to understand better the correlations between p_{d1} and p_{d2} . We consider the value of p_{d2} as a more appropriate and convenient one for numerical simulation of disordered samples in the context of EOT, and proposed a theoretical model which takes explicitly the disorder into account. Simulated spectra are in a good agreement with experimental ones. We have shown how the concurrence between nanopore depth and disorder level defines the quality of EOT excitation. We believe that our results, which reveal the possibilities of NPL for EOT-based applications, will pave the way toward plasmonic devices with a polycrystalline design.

ACKNOWLEDGEMENTS

The work was funded by the SIS 488 doctoral school of Saint-Etienne, university of Lyon (France), and by RFBR, project number 19-32-90034. The authors would like to thank CNRS engineers Marion HOCHEDÉL and Arnaud VALOUR for the technical support.

REFERENCES

- Andrew, P. and Barnes, W. (2004). Energy transfer across a metal film mediated by surface plasmon polaritons. *Science*, 306(5698):1002–1005.
- Avrutsky, I., Li, B., and Zhao, Y. (2000). Characterization of two-dimensional colloidal polycrystalline materials using optical diffraction. *JOSA B*, 17(6):904–909.
- Berthod, L., Shavdina, O., Vocanson, F., Langlet, M., Dellea, O., Veillas, C., Reynaud, S., Verrier, I., and Jourlin, Y. (2017). Colloidal photolithography applied to functional microstructure on cylinder based on photopatternable TiO_2 sol-gel. *Microelectronic Engineering*, 177:46–51.
- Bhawalkar, S. P., Qian, J., Heiber, M. C., and Jia, L. (2010). Development of a colloidal lithography method for patterning nonplanar surfaces. *Langmuir*, 26(22):16662–16666.
- Campos, L. M., Meinel, I., Guino, R. G., Schierhorn, M., Gupta, N., Stucky, G. D., and Hawker, C. J. (2008). Highly versatile and robust materials for soft imprint lithography based on thiol-ene click chemistry. *Advanced Materials*, 20(19):3728–3733.
- Cao, J., Sun, Y., Zhu, H., Cao, M., Zhang, X., and Gao, S. (2018). Plasmon-enhanced optical transmission at multiple wavelengths through an asymmetric corrugated thin silver film. *Plasmonics*, 13(5):1549–1554.
- Delléa, O., Shavdina, O., Fugier, P., Coronel, P., Ollier, E., and Désage, S.-F. (2014). Control methods in microspheres precision assembly for colloidal lithography.

- In Ratchev, S., editor, *Precision Assembly Technologies and Systems*, pages 107–117. Springer Heidelberg.
- Deng, Z.-L., Cao, Y., Li, X., and Wang, G. P. (2018). Multifunctional metasurface: from extraordinary optical transmission to extraordinary optical diffraction in a single structure. *Photonics Research*, 6(5):443–450.
- Ebbesen, T. W., Lezec, H. J., Ghaemi, H., Thio, T., and Wolff, P. A. (1998). Extraordinary optical transmission through sub-wavelength hole arrays. *Nature*, 391(6668):667–669.
- Ekşioğlu, Y., Cetin, A. E., and Petráček, J. (2016). Optical response of plasmonic nanohole arrays: comparison of square and hexagonal lattices. *Plasmonics*, 11(3):851–856.
- Fang, X., Lou, M., Bao, H., and Zhao, C. (2015). Thin films with disordered nanohole patterns for solar radiation absorbers. *Journal of Quantitative Spectroscopy and Radiative Transfer*, 158:145–153.
- Farcau, C. (2019). Metal-coated microsphere monolayers as surface plasmon resonance sensors operating in both transmission and reflection modes. *Scientific reports*, 9(1):1–9.
- Gartia, M. R., Hsiao, A., Pokhriyal, A., Seo, S., Kulsharova, G., Cunningham, B. T., Bond, T. C., and Liu, G. L. (2013). Colorimetric plasmon resonance imaging using nano lycurgus cup arrays. *Advanced Optical Materials*, 1(1):68–76.
- Genet, C. and Ebbesen, T. W. (2010). Light in tiny holes. In *Nanoscience And Technology: A Collection of Reviews from Nature Journals*, pages 205–212. World Scientific.
- Gray, A. T., Mould, E., Royall, C. P., and Williams, I. (2015). Structural characterisation of polycrystalline colloidal monolayers in the presence of aspherical impurities. *Journal of Physics: Condensed Matter*, 27(19):194108.
- Hahn, C., Hajebifard, A., and Berini, P. (2020). Helium focused ion beam direct milling of plasmonic heptamer-arranged nanohole arrays. *Nanophotonics*, 9(2):393–399.
- Jamiolkowski, R. M., Chen, K. Y., Fiorenza, S. A., Tate, A. M., Pfeil, S. H., and Goldman, Y. E. (2019). Nanoaperture fabrication via colloidal lithography for single molecule fluorescence analysis. *PloS one*, 14:10.
- Jourlin, Y., Tonchev, S., Tishchenko, A., Pedri, C., Veillas, C., Parriaux, O., Last, A., and Lacroute, Y. (2009). Spatially and polarization resolved plasmon mediated transmission through continuous metal films. *Optics express*, 17(14):12155–12166.
- Li, J.-Y., Hua, Y.-L., Fu, J.-X., and Li, Z.-Y. (2010). Influence of hole geometry and lattice constant on extraordinary optical transmission through subwavelength hole arrays in metal films. *Journal of Applied Physics*, 107(7):073101.
- Liu, J., Zhang, X., Li, W., Jiang, C., Wang, Z., and Xiao, X. (2020a). Recent progress in periodic patterning fabricated by self-assembly of colloidal spheres for optical applications. *Sci. China Mater.*, 63:1418–1437.
- Liu, Q., Song, Y., Zeng, P., Zhang, C., Chen, Y., Wang, H., Luo, Y., and Duan, H. (2020b). High-fidelity fabrication of plasmonic nanoholes array via ion-beam planarization for extraordinary transmission applications. *Applied Surface Science*, 526:146690.
- Lotito, V. and Zambelli, T. (2016). Self-assembly of single-sized and binary colloidal particles at air/water interface by surface confinement and water discharge. *Langmuir*, 32(37):9582–9590.
- Nau, D., Schönhardt, A., Bauer, C., Christ, A., Zentgraf, T., Kuhl, J., Klein, M., and Giessen, H. (2007). Correlation effects in disordered metallic photonic crystal slabs. *Physical review letters*, 98(13):133902.
- Park, J., Lee, H., Gliserin, A., Kim, K., and Kim, S. (2020). Spectral shifting in extraordinary optical transmission by polarization-dependent surface plasmon coupling. *Plasmonics*, 15(2):489–494.
- Pendergraph, S. A., Park, J. Y., Hendricks, N. R., Crosby, A. J., and Carter, K. R. (2013). Facile colloidal lithography on rough and non-planar surfaces for asymmetric patterning. *Small*, 9(18):3037–3042.
- Qu, C. and Kinzel, E. C. (2016). Polycrystalline metasurface perfect absorbers fabricated using microsphere photolithography. *Optics letters*, 41(15):3399–3402.
- Quint, S. and Pacholski, C. (2014). Getting real: Influence of structural disorder on the performance of plasmonic hole array sensors fabricated by a bottom-up approach. *Journal of Materials Chemistry C*, 2(36):7632–7638.
- Reilly III, T. H., Tenent, R. C., Barnes, T. M., Rowlen, K. L., and van de Lagemaat, J. (2010). Controlling the optical properties of plasmonic disordered nanohole silver films. *ACS nano*, 4(2):615–624.
- Richter, C., Schmiedeberg, M., and Stark, H. (2011). A colloidal model system with tunable disorder: Solid-fluid transition and discontinuities in the limit of zero disorder. *The European Physical Journal E*, 34(10):107.
- Rojas-Ochoa, L. F., Mendez-Alcaraz, J., Sáenz, J., Schurtenberger, P., and Scheffold, F. (2004). Photonic properties of strongly correlated colloidal liquids. *Physical review letters*, 93(7):073903.
- Ruan, W.-d., Lü, Z.-c., Nan, J., Wang, C.-x., Bing, Z., and Zhang, J.-h. (2007). Facile fabrication of large area polystyrene colloidal crystal monolayer via surfactant-free langmuir-blodgett technique. *Chemical Research in Chinese Universities*, 23(6):712–714.
- Sauvage-Vincent, J., Tonchev, S., Veillas, C., Reynaud, S., and Jourlin, Y. (2013). Optical security device for document protection using plasmon resonant transmission through a thin corrugated metallic film embedded in a plastic foil. *Journal of the European Optical Society-Rapid publications*, 8:1–6.
- Shavdina, O., Berthod, L., Kampfe, T., Reynaud, S., Veillas, C., Verrier, I., Langlet, M., Vocanson, F., Fugier, P., Jourlin, Y., and Dellea, O. (2015). Large area fabrication of periodic TiO₂ nanopillars using microsphere photolithography on a photopatternable sol–gel film. *Langmuir*, 31(28):7877–7884.
- Shcherbakov, A. A. and Tishchenko, A. V. (2017). Generalized source method in curvilinear coordinates for

- 2d grating diffraction simulation. *J. Quant. Spectrosc. Radiat. Transf.*, 187:76–96.
- Ushkov, A. A., Verrier, I., Kampfe, T., and Jourlin, Y. (2020). Subwavelength diffraction gratings with macroscopic moiré patterns generated via laser interference lithography. *Optics Express*, 28(11):16453–16468.
- Ushkov, A. A., Shcherbakov, A. A., Verrier, I., Kampfe, T., and Jourlin, Y. (2019). Systematic study of resonant transmission effects in visible band using variable depth gratings. *Scientific reports*, 9(1):1–9.
- Vogel, N., de Viguerie, L., Jonas, U., Weiss, C. K., and Landfester, K. (2011). Wafer-scale fabrication of ordered binary colloidal monolayers with adjustable stoichiometries. *Advanced functional materials*, 21(16):3064–3073.
- Wang, W., Peng, Y., and Cui, T. (2013). Simulation study of extraordinary optical transmission induced by subwavelength nanopore arrays towards label-free biochemical analysis. In *2013 International Conference on Manipulation, Manufacturing and Measurement on the Nanoscale*, pages 140–145. IEEE.
- Wen, K., Luo, X.-Q., Chen, Z., Zhu, W., Guo, W., and Wang, X. (2019). Enhanced optical transmission assisted near-infrared plasmonic optical filter via hybrid subwavelength structures. *Plasmonics*, 14(6):1649–1657.
- Yeh, W.-H., Petefish, J. W., and Hillier, A. C. (2011). Diffraction-based tracking of surface plasmon resonance enhanced transmission through a gold-coated grating. *Analytical chemistry*, 83(15):6047–6053.
- Yue, W., Wang, Z., Yang, Y., Li, J., Wu, Y., Chen, L., Ooi, B., Wang, X., and Zhang, X.-x. (2014). Enhanced extraordinary optical transmission (EOT) through arrays of bridged nanohole pairs and their sensing applications. *Nanoscale*, 6(14):7917–7923.
- Zhang, X., Li, Z., Ye, S., Wu, S., Zhang, J., Cui, L., Li, A., Wang, T., Li, S., and Yang, B. (2012). Elevated ag nanohole arrays for high performance plasmonic sensors based on extraordinary optical transmission. *Journal of Materials Chemistry*, 22(18):8903–8910.
- Zhang, Z., Geng, C., Hao, Z., Wei, T., and Yan, Q. (2016). Recent advancement on micro-/nano-spherical lens photolithography based on monolayer colloidal crystals. *Advances in colloid and interface science*, 228:105–122.
- Zhao, J., Yu, X., Yang, X., Xiang, Q., Duan, H., and Yu, Y. (2017). Polarization independent subtractive color printing based on ultrathin hexagonal nanodisk-nanohole hybrid structure arrays. *Optics express*, 25(19):23137–23145.
- Ziman, J. M. (1979). *Models of disorder: the theoretical physics of homogeneously disordered systems*. Cambridge University.